Path Planning for Wheel Loaders: a Discrete Optimization Approach

Beichuan Hong* and Xiaoliang Ma

***Abstract*—In construction projects, wheel loader is widely used for transporting building materials. The operations of wheel loader contain extensively repetitive tasks that could be optimized and automated for sustainable construction. This paper proposes, according to optimal control theory, an optimization approach for the loading cycle concerning fuel efficiency and environmental impacts. Based on a 2D space discretization and a detailed wheel loader model, a dynamic programming approach is formulated for optimal path search. The method is effective for integrating the system models with the path planning algorithm and for handling objective functions and constraints. A case study was carried out to demonstrate the application of the proposed algorithm for the loading cycle with spatial constraints.**

I. Introduction

Wheel loader is one type of heavy-duty vehicles that is widely used to transport building materials for short distance at construction sites. The loading cycle of such vehicle is composed of frequent and repetitive tasks: filling, lifting bucket, traveling to a location, dumping materials to the receiver, e.g. a haul truck, then returning to the pile [1]. Different from the bucket filling process [2], the transport process does not depend on the loading materials. The loading path between the pile and receiver could be optimized according to different objectives such as productivity, fuel efficiency or emissions. Fig. 1 depicts a trajectory (also named as "v-shape path") of the wheel loader including four steps:

- move backward to the reversing point with loads;
- reverse the gear and move forward to the receiver;
- move backward after dumping;
- return to the pile position for the next loading cycle.

Path planning for the loading trajectory has already been studied in literature. For instance, a recent paper by Alshaer et al [3] extended the optimal path generation approach proposed by Reeds and Shepp [4] for the loading operations of wheel loader. Meanwhile, Filla et al [5] investigated the loading patterns in addition to the conventional "V-shape" path. Moreover, a model predictive control based algorithm was proposed by Nayl et al for real-time motion planning of articulated vehicle [6].

The authors are with the System Simulation & Control Lab, Department of Transport Science, KTH Royal Institute of Technology. Teknikringen 10, 10044, Stockholm, Sweden.

This study is partly supported by the project "SCORE: Sustainable Construction Operations for Reduced Emissions" funded by Volvo CE and the Chinese Scholarship Council.

The corresponding email: beichuan@kth.se

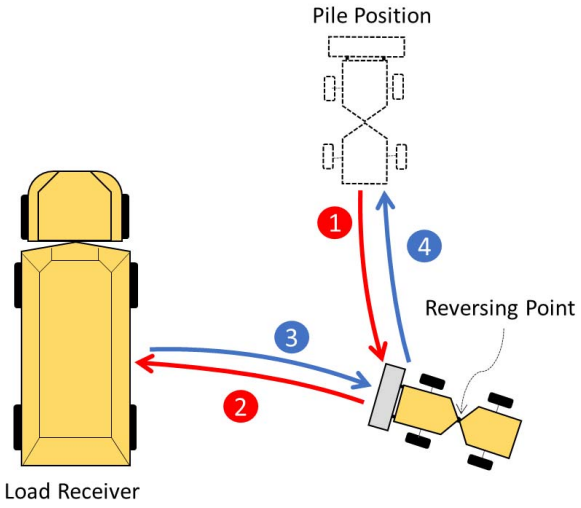

Figure 1. Trajectory of a wheel loader during the loading cycle.

Most of the studies mentioned above focus on collision avoidance or productivity. In order to evaluate fuel performance and emissions of wheel loader, detailed modeling of the mechanical system is important [7]. In this regard, Nezhadali and Eriksson [8][9] proposed an optimal control based approach for deriving loading path while modeling the energy usage by different components of the wheel loader system. The trade-off between fuel and production rate of the loading cycle is also analyzed. Nevertheless, the nonlinearity of high-dimension system could easily lead to a larger amount of computational cost, and the proposed optimization-based solver might also suffer from issues such as oscillation in the control system. Finally, there are also requirements to consider both fuel and vehicle emissions for optimal path planning.

This paper proposes to search the optimal path for the wheel loader operation using a discrete dynamic programming (DP) approach. The rest of the paper is organized as follows. Section II presents a detailed model of wheel loader. The optimal control problem is formulated in section III, where a space-based discrete DP algorithm is illustrated as a solution approach. Finally, section IV presents a detailed case that investigates the optimal trajectories in an earthmoving scenario.

978-1-5386-1526-3/17/$31.00 ©2017 IEEE

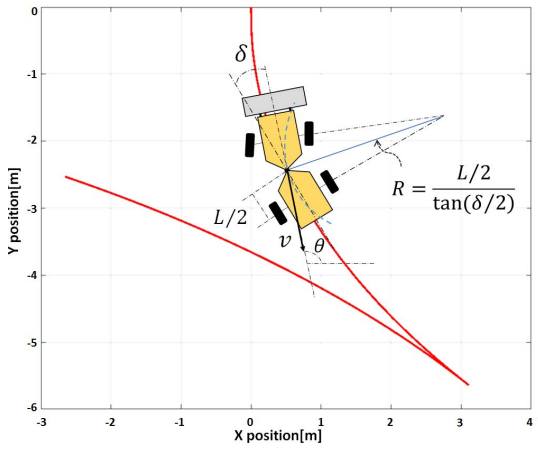

Figure 2. Kinematic model of the articulated vehicle.

Table I
PROPULSION SYSTEM PARAMETERS

Parameter	Description
P_{str}	Power consumption for steering
P_{trac}	Power consumption for traction
P_{lift}	Power consumption for lifting system
P_{loss}	Power loss during loading process
P_e^{max}	Engine power upper band
T_e	Engine torque
T_{brake}^{max}	Maximum braking torque
r_w	Wheel radius of loader
ω	Heading angular speed of loader
n_e	Engine speed
L	Length between front and rear axle
$\gamma_g, \gamma_f, \gamma_{tc}$	Ratios of gearbox, differential, and torque converter
m	Loader mass with full loading
I_e, I_s, I_w	Inertias of engine, propeller shaft, and wheels
v	Speed of wheel loader
a	Acceleration of wheel
β	Steering angular velocity

II. SYSTEM MODELING

The wheel loader model contains three parts: a kinematic model utilized to describe the motion of wheel loader; a propulsion system model for estimating the state and constraints of mechanical components; and finally an engine-based model of fuel consumption and emissions based on data from in-lab engine tests.

A. Kinematic model

Kinematic modeling of articulated vehicle has been utilized to describe the steering motion of construction machine. In the study of Nezhadali and Eriksson [8], a wheel loader is divided into a front body (tractor) and a rear body (trailer) linked by a free joint. Fig. 2 depicts the vehicle model with essential geometrical variables in the 2D plane. The motion of wheel loader is determined by the turning radius R as the radius of current translational velocity v. The steering angle δ is the difference between angles of front and rear parts. The steering angle velocity β is controlled within steering bounds. The relationship between steering angular velocity β and heading angular speed ω can be represented by

$$\dot{\theta}(t) = \omega(t) = \sigma(t)v(t) \tag{1}$$

$$\sigma(t) = \frac{1}{R(\delta(t))} = \frac{2\tan\frac{\delta(t)}{2}}{L} \tag{2}$$

$$\dot{\delta}(t) = \beta(t) \tag{3}$$

$$|\beta(t)| \leq \beta_{max} \tag{4}$$

where L is the length from loader's front wheel to the rear one, and the path curvature σ is used as the steering function by heading angle of front wheel ω. The wheel loader position (x, y) at time t is determined by the steering dynamics :

$$x(t) = x_0 + \int_{t_0}^{t} v(t)\cos(\theta(t))\,\mathrm{d}t \tag{5}$$

$$y(t) = y_0 + \int_{t_0}^{t} v(t)\sin(\theta(t))\,\mathrm{d}t \tag{6}$$

where (x_0, y_0) is the initial position, and the speed v and heading angle θ are limited by the mechanical constraints of the wheel loader.

B. Propulsion system model

The propulsion system of a wheel loader consists of diesel engine, automatic transmission, hydraulic arm, drive shaft and so on. Fig. 3 illustrates the main parts of the propulsion system and the relations among them. Table I summarizes the parameters to describe the dynamics of the propulsion system during the loading process. The transient dynamics of wheel loader is shortly presented in this section.

The power usage of the wheel loader is modeled by the following equations:

$$P_{out} = P_{trac} + P_{str} + P_{lift} + P_{loss} \tag{7}$$

$$P_{trac} = c_r.\ v.\ m_{total}.\ g \tag{8}$$

$$P_{str} = c_p.\ \beta^2 \tag{9}$$

$$P_{loss} = h(n_e/v, \dot{\omega}, \gamma_d, T_e) \tag{10}$$

The engine output power P_{out} is mainly divided into: the traction power P_{trac}, steering power P_{str}, lifting power P_{lift}, and the rest is categorized as the energy losses P_{loss} through loading operations. Maps from the manufacturer are used for looking-up the values of P_{loss}. The lifting power P_{lift} here is independent from the loading path. In our study, P_{lift} is set using the average value of data from field tests in which the loader lifts a full-loading bucket to a specific height. Coefficients c_r, c_p are used for the power estimation. The propulsion system model presented here is calibrated using data from both the manufacturer and in-lab tests.

Essentially, the power flow of loading cycle can be calculated based on the dynamic model of loader components. The energy that drives the kinematics described by the equation (1) – (6) is constrained by the real-time power distribution in the propulsion system. Therefore, we can derive the motion boundaries as a result of power balance. In the following

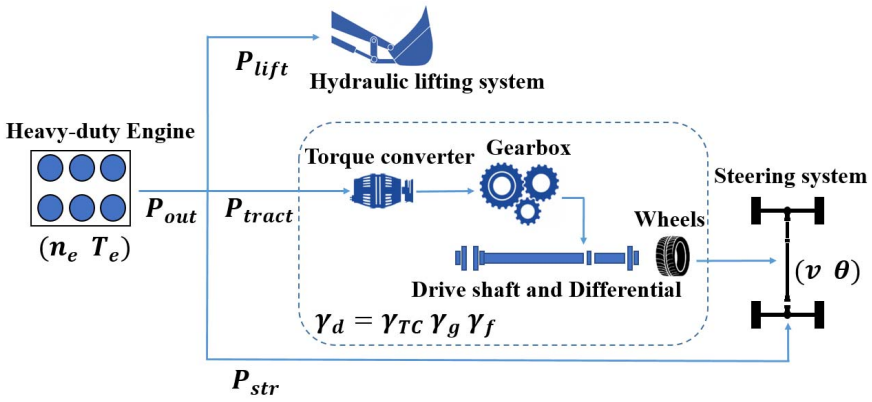

Figure 3. Structure of propulsion system model based on the power distribution of a wheel loader.

equations, the limitation values on acceleration a and angular acceleration $\dot{\omega}$ are derived as the motion constraints:

$$a_{max} = \frac{P_e^{max} - P_{out}}{n_e\ r_w\ m_{tot}} \tag{11}$$

$$a_{min} = -\frac{P_{trac}\ + r_w\ T_{brake}^{max}}{n_e\ r_w\ m_{tot}} \tag{12}$$

$$\dot{\omega}_{max} = \frac{\beta_{max}(v^2 + L^2\omega^2/4)}{Lv} + \frac{a\omega}{v} \tag{13}$$

$$\dot{\omega}_{min} = -\frac{\beta_{max}(v^2 + L^2\omega^2/4)}{Lv} + \frac{a\omega}{v} \tag{14}$$

where the maximum engine power output $P_e^{max}(n_e)$, also known as "engine performance curve" denotes the power upper bound according to n_e. The maximum brake torque T_{brake}^{max} is a constant parameter for a specified loader. The inertia of components is involved and leads to the equivalent total mass as follows:

$$m_{tot} = m + \frac{I_e/\gamma_d^2 + I_s/\gamma_f + I_w}{r_w^2} \tag{15}$$

and the torque is calculated by the engine power output and engine speed:

$$T_e = \frac{P_{out}}{n_e} \tag{16}$$

$$n_e = \frac{\gamma_d\ v}{r_w} \tag{17}$$

where γ_d in (18) represents the product of all speed ratios of the driveline i.e.,

$$\gamma_d = \gamma_g\ \gamma_f\ \gamma_{tc} \tag{18}$$

$$\gamma_{tc} = g(n_e/v, a) \tag{19}$$

The gearbox ratio γ_g is fixed after the gear shifting, whereas the ratio of torque converter γ_{tc} is defined by the characteristics of the fluid coupling device.

C. Engine-based fuel and emission estimation

This study employs an engine-based approach [10] to calculate the fuel economy and engine-out emissions of wheel loader. Data from manufacturers are utilized to generate fuel and emission maps depending on engine speed n_e (rad/s) and torque T_e (Nm). Moreover, the results of in-lab engine tests, e.g. NRTC (Non-road Transient Cycle) and ETC (European Transient Cycle), are used to calibrate the map-based model in different operational arranges. For the LW321F wheel loader evaluated in the later case study, the modeling results of the common rail turbo-charged diesel engine are validated by real tests. The engine-based approach shows a good accuracy when compared with transient tests.

The accuracy of emission map is highly affected by the transient operations. A calibration model ψ' is added to deal with the error due to transient working conditions. The model incorporates the changes of engine rotational speed Δn_e and torque ΔT_e as inputs, i.e.,

$$\psi = \psi_{map}(n_e, T_e) + \psi'(\Delta n_e, \Delta T_e) \tag{20}$$

and the instantaneous NOx emission (mg/s) was modeled in our previous study [10].

III. Optimal Path Planning

A. Optimal control formulation

This paper solves the path planning of wheel loader during the loading cycle using the optimal control theory. It is known that the general optimal control problem can be formulated by the following ODE system:

$$\begin{cases} \dot{\mathbf{x}}(t) = \mathbf{f}(\mathbf{x}(t), \mathbf{u}(t)) & t \geq 0 \\ \mathbf{x}(0) = \mathbf{x}_0 \end{cases} \tag{21}$$

where $\mathbf{x}(t)$ is the state of system controlled and $\mathbf{u}(t)$ is the control input at time t. The initial boundary condition is given by $\mathbf{x}_0$.

One early study derives optimal vehicle trajectory by solving the two point boundary value problem (BVP) in which the final state $\mathbf{x}(T) = \mathbf{x}_T$ is known and the control period T is free [11]. The control objective is to minimize certain impact measures, fuel consumption or emission for example, represented by

$$J(\mathbf{u}) = \int \phi\big(\mathbf{x}(t), \mathbf{u}(t)\big)dt \tag{22}$$

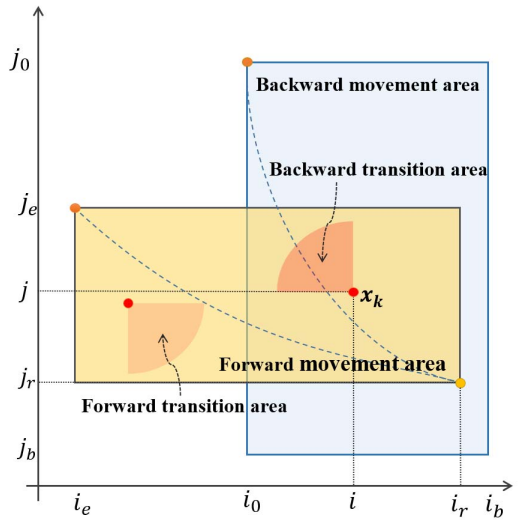

Figure 4. Illustration of the backward and forward movements in the discretized working area. The lower right corner (i_b, j_b) of the backward area is specified according to the construction scenario.

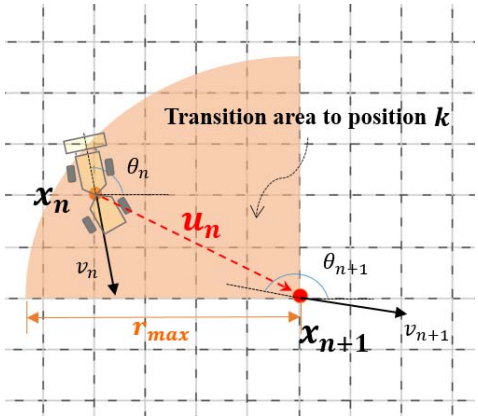

Figure 5. An example of the state transition at kth position for the backward movement.

where $\phi(\mathbf{x}(t), \mathbf{u}(t))$ is instantaneous cost function. The basic problem is to solve the optimal control $\mathbf{u}^*(\cdot)$ for minimizing the cost function i.e.

$$J(\mathbf{x}^*, \mathbf{u}^*) = \min_{\mathbf{u}\in\mathbf{U}} J(\mathbf{x}, \mathbf{u}). \tag{23}$$

where $\mathbf{x}^*$ is the optimal intermediate system states.

We use the similar formulation above in the optimal path planning for wheel loader in the loading process described before. The control objective function is generally written as follows:

$$J(\mathbf{u}) = \int \Big\{1 + \lambda_1 \phi\big(\mathbf{x}(t), \mathbf{u}(t)\big) + \lambda_2 \psi\big(\mathbf{x}(t), \mathbf{u}(t)\big)\Big\} dt \tag{24}$$

where $\phi(\mathbf{x}(t), \mathbf{u}(t))$ and $\psi(\mathbf{x}(t), \mathbf{u}(t))$ are the instantaneous cost function for fuel and emission respectively. In addition, the operational time is also added as a measure for productivity. λ_1 and λ_2 are constants that need to be determined. The solution is different for different λ_1 and λ_2.

In our solution practice, the constrained optimization problem is however formulated as follows:

$$J(\mathbf{u}) = \int \phi\big(\mathbf{x}(t), \mathbf{u}(t)\big) dt \tag{25}$$

s.t.

$$\begin{aligned} \int \psi(\mathbf{x}(t), \mathbf{u}(t)) dt \Big/ T &\leq \bar{\Psi}_{max} \\ T &\leq T_{max} \end{aligned}$$

where Ψ_{max} and T_{max} are constraint constants. In addition, the system models and boundary conditions are also part of the formulation.

B. Space-based dynamic programming model

The fuel consumption is not a convex function and the vehicle model is nonlinear and high dimensional. Specifically, the loading process contains both a backward and a forward movement. Machine has to accelerate and brake several times and the states of the loader are discontinuous e.g. gearbox ratios and dynamic acceleration constraints.

It is natural to extend the discrete space-based DP approach derived in [11] in the 2D grid space. The grid nodes on the discretized working area Ω in this study are represented by the coordinate (i, j) with δx and δy as the unit length. Without loss of generality, this paper assumes the location of receiver is on the left side of the material pile. Fig 4 shows an example of discretized work zone (starting point (i_0, j_0) and ending point (i_e, j_e)) with backward and forward movement areas in a loading process. While the dimensions of the state and control input are significantly increased, the DP recursion model can be still formulated abstractly as follows:

$$\begin{aligned} J(n, \mathbf{x}_n) &= \min_{\mathbf{u}\in\mathbf{U}(n,\mathbf{x}_n)} \{\phi_n(\mathbf{x}_n, \mathbf{u})\Delta t_n + J(n+1, \mathbf{x}_{n+1})\} \\ & n = N-1, ..., 0 \end{aligned} \tag{26}$$

s.t.

$$\begin{aligned} \mathbf{x}_{n+1} &= \mathbf{f}(n, \mathbf{x}_n, \mathbf{u}_n);\ \mathbf{x}_n \in \mathbf{X};\ \mathbf{u}_n \in \mathbf{U} \\ \Psi_n / \Delta t_n &\leq \hat{\psi}_{max} \\ \sum \Delta t_n &\leq T_{max} \end{aligned}$$

where n is the iteration index, and the initial state $\mathbf{x}_0$ is given. $\mathbf{X}$ denotes the state space while the set of admissible control variables $\mathbf{U}$ is determined by the current state $\mathbf{x}_n$. Noticeably, instantaneous emission rate ψ_n is regulated by $\hat{\psi}_{max}$ for each step.

C. Discretized vehicle dynamics model

In order to implement the DP model, the vehicle dynamics should be represented for discretized space (see Fig.5). Vehicle state depends not only on position but also heading angle. To reduce the index number, a transformation is implemented to project the 2D map (i, j) into an array with index k. Moreover, due to various potential trajectories with different speed profiles and heading angles, a wheel loader

could have many states at one location k. Hence, in the implemetation, the vehicle state vector at position k, or (i, j), can be expressed by

$$\mathbf{x}_{k,q} = [v_{k,q}\ \theta_{k,q}]^T \quad \mathbf{x}_{k,q} \in \mathbf{X}_k \tag{27}$$

where $\mathbf{X}_k$ is the state space at position k. The index q is used to represent the qth vehicle state at position k. $v_{k,q}$ and $\theta_{k,q}$ are the velocity and heading angle.

Assume that at the stage n vehicle moves from step n (pth state at position h) to step $n+1$ (qth state at position k):

$$\mathbf{x}_{n+1} = f(\mathbf{x}_n, \mathbf{u}_n) \tag{28}$$

where the control vector $\mathbf{u}_n \in \mathbf{U}(\mathbf{x}_n)$. When the control input is only set as the speed change, i.e.

$$\mathbf{u}_n = \Delta v_n, \tag{29}$$

we can derive the state transition as follows:

$$\Delta\theta_n = \frac{(2v_n + \Delta v_n)(\Delta y_n \cos\theta_n - \Delta x_n \sin\theta_n)}{v_n(\Delta x_n \cos\theta_n + \Delta y_n \sin\theta_n)} \tag{30}$$

$$\Delta t_n = \frac{2\Delta y_n}{(2v_n + \Delta v_n)\sin\theta_n + v_n \cos\theta_n \Delta\theta_n} \tag{31}$$

$$a_n = \frac{\Delta v_n}{\Delta t_n} \tag{32}$$

$$\omega_n = \frac{\Delta\theta_n}{\Delta t_n} \tag{33}$$

where a_n and ω_n are the acceleration and heading speed during the transition respectively.

According to vehicle system modeling, the state and control variables are regulated by dynamic characteristics of the loader and lead to the following constraints:

$$\dot{\omega}_n^{min}(v_n)\Delta t_n \le \omega_n \le \dot{\omega}_n^{max}(v_n)\Delta t_n \tag{34}$$

$$a_n^{min}(\mathbf{x}_n) \le a_n \le a_n^{max}(\mathbf{x}_n) \tag{35}$$

$$\psi_n \le \hat{\psi}_{max} \tag{36}$$

$$v_{min} \le v_{n+1} \le v_{max} \tag{37}$$

$$\theta_{min} \le \theta_{n+1} \le \theta_{max}. \tag{38}$$

D. Forward search algorithm

In practice, the backward DP model represented by equation (26) cannot be implemented directly mainly because the loading process is not continuous and includes two procedures connected by a reverse point. Therefore, we implement a forward recursion to generate all potential states. The optimal path could be found when all possible states are explored.

A more detailed description of the forward search algorithm is illustrate by Algorithm 1. Starting with initial state $\mathbf{x}_o$, the states at each grid node in the explored area are generated and stored in a database $\mathbf{S}^b$ with respect to their positions. Nodes in the backward movement area with state of speed being zero are taken as the potential reversing point (i_r, j_r), which is also the possible starting point for generating the forward movement in another database $\mathbf{S}^f$. Since all finial states with speed being zero and heading angles within a certain range are possible candidate for the final state, $\mathbf{X}^e$ is introduced to represent admissible finial states at (i_e, j_e). When all possible states are generated, the optimal trajectory can be derived by applying the backward DP recursion in equation (26). But in our implementation, the paths and corresponding costs are all stored while states are generated. The backward process is indeed unnecessary.

Algorithm 1 Discrete approach for optimal loading path

Input: initial state $\mathbf{x}_o$, working area configuration Ω, allowed states space $\mathbf{X}^e$ at final position.

Output: optimal policy π^*, optimal cost-to-go J^*, state database $\mathbf{S}$.

$\mathbf{S}^b \leftarrow states\_exploration(\mathbf{x}_o, (i_b, j_b))$
for all $\mathbf{x} \in \mathbf{S}^b$ **do**
  if $v = 0$ **then** ▷ vehicle state with zero-speed
    $\mathbf{S}^f \leftarrow states\_exploration(\mathbf{x}, (i_e, j_e))$
$\mathbf{S} \leftarrow \mathbf{S}^f + \mathbf{S}^b$
for all $\mathbf{x} \in \mathbf{X}^e$ at position (i_e, j_e) **do**
  $\hat{J}^*(\mathbf{x}, N) \leftarrow 0$
  for $n \leftarrow N, 1$ **do**
    $\hat{J}^*(n, \mathbf{x}) = \min_{\mathbf{u}\in\mathbf{U}(n,\mathbf{x})} \{\phi_n(\mathbf{x}, \mathbf{u})\Delta t_n + \hat{J}(n+1, \mathbf{x})\}$
    $\hat{\pi}^*(n, \mathbf{x}) = \operatorname{argmin}_{\mathbf{u}\in\mathbf{U}(n,\mathbf{x})} \{\phi_n(\mathbf{x}, \mathbf{u})\Delta t_n + \hat{J}(n+1, \mathbf{x})\}$
  if $\hat{J}^* < J^*$ **then**
    Update J^* and π^*

Some essential efforts are put to reduce the computational cost. During the space-based states exploration, each motion state $\mathbf{x}_{k,q}$ is produced by previous state $\mathbf{x}_{h,p}$ whose position h is located before the current position k. Obviously, the state transitions of backward and forward have opposite moving directions. Since the calculation of state transitions between impractical distances leads to unnecessary computational cost, the admissible transition area of position k, light red area in Fig.5, is derived for enhancing the computational efficiency. The parameter r_{max} is the maximum allowed distance between two consecutive states. The value of r_{max} is set based on the maximum allowed speed in the specified construction scenarios. Assume position h is in the admissible transition area of position k, thus the longitude and latitude distances Δx_h and Δy_h are following: $\sqrt{\Delta x_h^2 + \Delta y_h^2} \le r_{max}$.

IV. Numerical example

In this section, the discrete optimization approach is implemented for demonstrating how much potential benefit the optimal planning may bring in real application. A LW321F type wheel loader has been employed for performing earthmoving task with sensors for measuring both vehicle signals and engine-out emission. A total of 763 full-bucket loading cycles is completed with the same starting and end positions in the field test, and operational data collected from the real-world earthmoving operations are used for model calibration and path analysis.

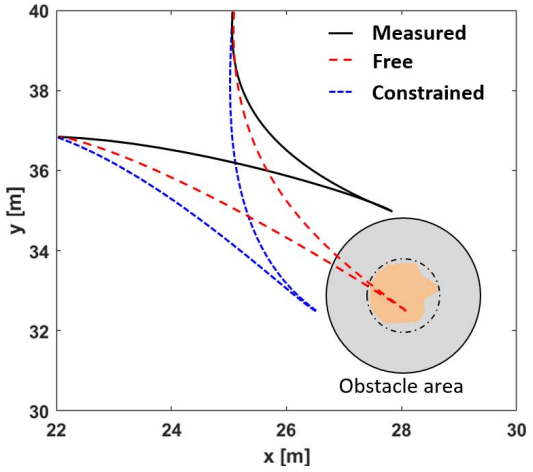

Figure 6. Trajectories based on the configuration of field tests and the working area is discretized as 81×81 for space-based optimization.

Table II
RESULTS OF THE OPTIMAL PATHS PER ONE CYCLE.

	Unit	**Measured**	**Constrained**	**Free**
Fuel usage	*g*	9.32	7.97	7.44
NOx emission	*mg*	172	166	162
Time	s	14.7	11.8	15.5
Production rate	*ton/s*	0.225	0.271	0.213

The loading cycle with lowest fuel consumption is picked from the measurement data, and the corresponding trajectory is plotted in Fig. 6 using black solid line. Then, two optimal trajectories are proposed by our optimization approach for minimizing the environmental impacts of the earthmoving task. The first numerical experiment shows the free optimal path (plotted as red dashed line) without any working area limitation. However, based on the scenario in the construction site, a rock pile needs to be considered as the obstacle on working space. Due to the driving safety, the length of wheel loader's tailer needs be considered for obstacle avoidance. Therefore, the obstacle area in path planning is mark as a circle area (gray area in Fig. 6) by involving a safe distance. After the location indexes inside the obstacle area are excluded from the state database, the constrained optimal path (blue dashed line) is calculated via Algorithm 1.

Compared with the measured data, the constrained optimal path obviously reduces the fuel consumption by 14% in one loading cycle meanwhile the NOx pollutant also decreases to 166 mg/cycle under the emission constraint. The time cost of the loading cycle is reduced due to a high speed profile suggested by the optimization approach. The free optimal path gets the lowest fuel consumption and NOx emission by adopting high vehicle speed and smooth acceleration. On the other hand, the production rate of the free optimal path is slimly lower than the measured one as shown in Table II.

V. SUMMARY AND FURTHER PERSPECTIVES

This paper proposes a discrete optimization approach to solve the optimal path planning problem by integrating the dynamics model of wheel loader with the optimal control theory. Using a spatial dynamic programming formulation, the optimal trajectory of the wheel loader is derived for minimal fuel and emission during the loading process. The method is demonstrated by numerical experiments based on an earthmoving scenario. The discrete optimization approach shows flexibilities for integrating with system models and handling optimization objectives and constraints. Nevertheless, several aspects still require further investigation. For example, the influence of the discretization step needs an in-depth examination for defining a reasonable range of control inputs. Also, the calculation of the wheel loader states by in Algorithm 1 is computationally expensive. In further work, we could separate this step as a pre-computed database for a real-time implementation. Furthermore, the optimization approach could be developed into an operator assistance system, or guide for sustainable autonomous construction vehicle operations. To this aim, it is important to also consider higher levels of detail with respect to the topographical characteristics of the construction site as well as interactions with other vehicles.

REFERENCES

[1] T. Samuelsson, R. Filla, B. Frank, and L. Skogh, "Selecting representative working cycles from large measurement data sets," *CVT 2016 Commercial Vehicle Technology Symposium*, 2016.
[2] R. Filla, M. Obermayr, and B. Frank, "A study to compare trajectory generation algorithms for automatic bucket filling in wheel loaders," in *3rd Commercial Vehicle Technology Symposium*, 2014, pp. 588–605.
[3] B. Alshaer, T. Darabseh, and M. Alhanouti, "Path planning, modeling and simulation of an autonomous articulated heavy construction machine performing a loading cycle," *Applied Mathematical Modelling*, vol. 37, no. 7, pp. 5315–5325, 2013.
[4] J. Reeds and L. Shepp, "Optimal paths for a car that goes both forwards and backwards," *Pacific journal of mathematics*, vol. 145, no. 2, pp. 367–393, 1990.
[5] R. Filla, "Optimizing the trajectory of a wheel loader working in short loading cycles," in *13th Scandinavian International Conference on Fluid Power; June 3-5; 2013; Linköping; Sweden*, no. 92. Linköping University Electronic Press, 2013, pp. 307–317.
[6] T. Nayl, G. Nikolakopoulos, and T. Gustafsson, "Effect of kinematic parameters on mpc based on-line motion planning for an articulated vehicle," *Robotics and Autonomous Systems*, vol. 70, pp. 16–24, 2015.
[7] T. Nilsson, A. Fröberg, and J. Åslund, "Predictive control of a diesel electric wheel loader powertrain," *Control Engineering Practice*, vol. 41, pp. 47–56, 2015.
[8] V. Nezhadali and L. Eriksson, "Optimal lifting and path profiles for a wheel loader considering engine and turbo limitations," in *Optimization and Optimal Control in Automotive Systems*. Springer, 2014, pp. 301–324.
[9] V. Nezhadali, B. Frank, and L. Eriksson, "Wheel loader operation - optimal control compared to real drive experience," *Control Engineering Practice*, vol. 48, pp. 1–9, 2016.
[10] B. Hong, X. Ma, H. Chen, and L. Lv, "Modeling of dynamic nox emission for nonroad machinery: a study on wheel loader using engine test data and on-board measurement," in *Transportation Research Board 95th Annual Meeting, Washington D.C.*, 2016.
[11] X. Ma, "Optimal controls of fleet trajectories for fuel and emissions," in *Intelligent Vehicles Symposium (IV), 2013 IEEE*. IEEE, 2013, pp. 1059–1064.